Thermo-mechanical Behaviors of Functionally Graded Shape Memory Alloy Timoshenko Composite Beams

ZHOU Bo[1], *KANG Zetian*[1], *MA Xiao*[1], *XUE Shifeng*[1*], *YANG Jie*[2]

1. College of Pipeline and Civil Engineering, China University of Petroleum (East China), Qingdao 266580, P. R. China;
2. School of Engineering, RMIT University, Melbourne 3083, Australia

(Received 26 November 2020; revised 21 January 2021; accepted 2 February 2021)

Abstract: This paper focuses on the thermo-mechanical behaviors of functionally graded (FG) shape memory alloy (SMA) composite beams based on Timoshenko beam theory. The volume fraction of SMA fiber is graded in the thickness of beam according to a power-law function and the equivalent parameters are formulated. The governing differential equations, which can be solved by direct integration, are established by employing the composite laminated plate theory. The influences of FG parameter, ambient temperature and SMA fiber laying angle on the thermo-mechanical behaviors are numerically simulated and discussed under different boundary conditions. Results indicate that the neutral plane does not coincide with the middle plane of the composite beam and the distribution of martensite is asymmetric along the thickness. Both the increments of the functionally graded parameter and ambient temperature make the composite beam become stiffer. However, the influence of the SMA fiber laying angle can be negligent. This work can provide the theoretical basis for the design and application of FG SMA structures.

Key words: shape memory alloy (SMA); shear deformation; thermal effect; laminated plate theory; functionally graded (FG) beam

CLC number: O343.5 **Document code:** A **Article ID:** 1005-1120(2021)01-0029-15

0 Introduction

In the last decade, functionally graded (FG) materials have been emerged and widely used to satisfy special features in engineering designs. Due to continuously changing material properties, FG materials have striking advantages over traditional homogeneous materials, such as high fracture toughness, improved stress distribution, the superior stress relaxation, capabilities of withstanding high temperatures, and large thermal gradients[1-3]. Shape memory alloys (SMAs) are a unique group of materials that have the ability to recover their original shapes from large deformations well beyond their elastic strain limits, owing to its reversible martensitic transformation. The deformation recovery may occur spontaneously upon unloading or be delayed until the material is heated to a certain temperature. The former behavior is referred to as pseudo-elasticity and the latter is referred to as the shape memory effect[4-8]. These unique properties have rendered the alloys wide use in a range of engineering applications, such as structural design[9], biomedicine[10] and micro electromechanical systems (MEMS)[11].

To meet the requirement of complex engineering applications, it is desirable to create FG SMAs in the specific direction[12]. FG SMAs would be considered as composites with smooth interfaces[13] that are capable of both suffering from lager recoverable deformation because of the pseudo-elasticity of the SMA phase and exhibiting better controllability of metal phase to guarantee the structural stability. Thanks to the extraordinary characteristics of FG

*Corresponding author, E-mail address: sfeng@upc.edu.cn.

How to cite this article: ZHOU Bo, KANG Zetian, MA Xiao, et al. Thermo-mechanical behaviors of functionally graded shape memory alloy Timoshenko composite beams[J]. Transactions of Nanjing University of Aeronautics and Astronautics, 2021,38(1):29-43.

http://dx.doi.org/10.16356/j.1005-1120.2021.01.003

SMAs, many researchers have been motivated to fabricate different kinds of FG SMAs and test their mechanical and transformation behaviors experimentally. For instance, Fu et al.[14] used the magnetron sputtering system to improve the hardness and tribological properties of NiTi-based SMA film by surface treatment. Mahmud et al.[15] created the FG near-equiatomic NiTi SMA by anneal within a temperature grade after cold work. Tian et al.[16] fabricated the multilayer FG NiTi films by the D. C. sputtering method. Employing the temperature sensitivity of phase transition and thermodynamic properties of SMA, several methods for manufacturing FG SMA have been put forward, such as laser irradiation[17], temperature gradient-anneal[18] and surface laser annealing method[19-20]. Yang et al.[21] experimentally and numerically analyzed the temperature profile of a Ti-45Ni-5Cu (at%) alloy wire generated by the Joule heating treatment. Meng et al.[22-23] created compositionally graded NiTi thin plates by utilizing the surface diffusing method. Shariat et al.[24] presented the fabrication and analytical solutions of FG SMA wires with transformation stress and strain grades. They also made experimental and theoretical investigations on the pseudo-elastic response of several geometrically graded NiTi SMA bars/strips at different stages of loading cycle[25-26]. Mohri et al.[27-28] created FG NiTi bi-layer thin film structures by RF magnetron sputter deposition incorporated with vacuum arcre-melting and annealing technologies, and experimentally investigated their mechanical and phase transformation behaviors. Liu et al.[29] created the FG SMA cylinder using different heat treatment processes and described its phase transformation behaviors. On the basis of previous work, Shariat et al.[30-31] reported the concept, design and experimentation of different types of FG NiTi alloys as well as various fabrication techniques. They also experimentally investigated their deformation behaviors under different thermo-mechanical loads[32]. Khaleghi et al.[33] produced a compositionally graded high temperature SMA by diffusion annealing of palladium into NiTi alloys with different chemical compositions and investigated their shape recovery properties on both micro and macro scales experimentally.

The mechanical behaviors of SMA composite structures subjected to complex loads have been described and predicted through theoretical analysis. For instance, Shariyat et al.[34] studied the eccentric impact behavior of SMA wire reinforced composite plates using composite laminate plate theory. Samadpour et al.[35] investigated the nonlinear free vibration behavior of composite plates embedded with SMA wire by the extended polycrystalline micromechanics method and composite laminate plate theory. Kamarian et al.[36] analyzed the thermal buckling behavior of SMA wire reinforced composite plates and presented the optimal design method. Soltanieh et al.[37] studied the impact behavior of SMA fiber reinforced composite laminates and developed the corresponding numerical calculation program.

The abovementioned studies focus on the SMA composite structures without considering the graded distribution of material parameters, material component and geometrical dimension. With the rapid increase of requirement for FG SMAs in the high and new technology field, it is urgent to comprehensivly understand the mechanical and transformation properties of FG SMA structures, and to describe their constitutive relations correctly. In recent years, the analytical solution for FG SMA structures has been taken up by many researchers. For examples, Shariat et al.[38] analytically described the deformation behavior of property graded NiTi plates subjected to the thermal-mechanical loads. Liu et al.[39] analytically described the thermal-mechanical behavior of the FG SMA composite subjected to thermal loading. Liu et al.[40] analytically solved the mechanical and phase transformation problems of FG SMA composites with Young's modulus and the thermal expansion coefficient varying along the thickness direction subjected to the thermo-mechanical coupling. Liu et al.[29] created a FG SMA cylinder and derived the analytical solution to predict its mechanical behaviors. Xue et al.[41] proposed a constitutive model to describe the mechanical behaviors of the FG porous SMA and applied the constructed model to the finite element calculation of the FG porous SMA cylinder. Asadi et al.[42] investigated the

nonlinear thermal instability of FG SMA sandwich plates subjected to a moving speed based on the geometrically nonlinear third-order deformation theory. Liu et al.[43] investigated the stress-induced phase transformation in geometrically graded SMA layers.

To the authors' knowledge, no previous study on the bending behaviors of transverse FG SMA composite beams considering the shear deformation and thermal effect has been reported in the open literature, although it is an important issue. Therefore, the main goal of this paper is to investigate the thermo-mechanical behaviors of FG SMA composite Timoshenko beams with volume fraction of SMA fiber varying along the thickness. To accomplish this, the nonlinear transformation evolution law of SMA is simplified to be linear, and the equivalent parameters of the FG SMA composite beam is obtained by the extended multi-cell micromechanics approach. The governing differential equations are established by the composite laminate plate theory. For further investigation, FG SMA composite beams with simply supported and clamped-free boundary conditions are numerically simulated. The influence of FG parameter, ambient temperature and SMA fiber laying angle on the thermo-mechanical behaviors of the FG SMA composite beams are discussed in detail. This work can provide a theoretical guidance and basis for the design and application of smart beam structures in the relevant field.

1 Simplified Constitutive Law of SMA

The constitutive law of the SMA fiber and the SMA-matrix mixture must be derived before deploying the governing equations of the FG SMA composite beam.

In order to replace experimental results for SMA behavior, certain constitutive models were developed.[44-45] As the phase variance in SMA are related to the axis of loading, SMAs are utilized predominantly in one-dimensional form. As shown in Fig. 1, based on the thermo-mechanical model deposed by Zhou et al.[45] for SMAs, the corresponding pseudo-elastic stress-strain relation with the thermal strain can be given as

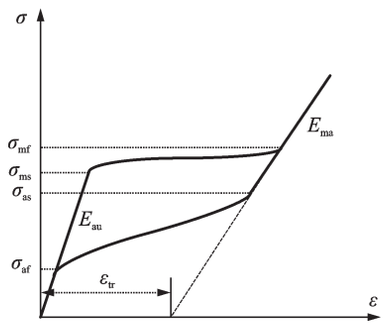

Fig.1 Stress-strain curves of SMA during the loading process

$$\sigma = E_F(\varepsilon - \alpha_F \Delta T - \eta \xi \varepsilon_{tr}) \tag{1}$$

where σ is the uniaxial stress; ε the uniaxial strain; η the loading direction coefficient with $\eta = 1$ for tensile state while $\eta = -1$ for compressive state; ξ the martensitic volume fraction; ε_{tr} the maximum transformation strain; and ΔT the temperature increment. Based on the rule of mixtures, the Young's modulus E_F and thermal expansion coefficient α_F of SMA fiber can be expressed as

$$E_F = \xi E_{ma} + (1-\xi) E_{au} \tag{2}$$

$$\alpha_F = \xi \alpha_{ma} + (1-\xi) \alpha_{au} \tag{3}$$

where the subscripts "ma" and "au" stand for martensite and austenite phases, respectively.

For the sake of simplicity, the nonlinear phase transformation evolution law of SMA during the loading process is simplified to be linear, and the martensitic volume fraction ξ during the direct transformation process can be described as follows

$$\xi = \frac{\varepsilon_{eq} - \varepsilon_{ms}}{\varepsilon_{mf} - \varepsilon_{ms}} \quad \varepsilon_{ms} \leqslant \varepsilon_{eq} \leqslant \varepsilon_{mf} \tag{4}$$

$$\varepsilon_{ms} = \frac{\sigma_{ms}}{E_{au}} \quad \varepsilon_{mf} = \frac{\sigma_{mf}}{E_{ma}} + \varepsilon_{tr} \tag{5}$$

where ε_{ms} and σ_{mf} are the martensite starting and the finishing strains, respectively. According to Brinson[44], the martensite starting stress σ_{ms} and the finishing stress σ_{mf} during the direct transformation process can be expressed as

$$\begin{cases} \sigma_{ms} = \sigma_{scr} + C_{ma}(T - M_s) \\ \sigma_{mf} = \sigma_{fcr} + C_{ma}(T - M_s) \end{cases} \tag{6}$$

where σ_{scr}, σ_{fcr}, T, M_s and C_{ma} are the initial values of the martensite starting and the finishing stresses, the temperature, the martensite starting temperature and the stress influence coefficient of martensite phase, respectively. The equivalent strain can be

given as [40]

$$\varepsilon_{eq}=\sqrt{\frac{2}{3}\left(\varepsilon_{ij}-\frac{1}{3}\varepsilon_{kk}\delta_{ij}\right)\left(\varepsilon_{ij}-\frac{1}{3}\varepsilon_{kk}\delta_{ij}\right)} \tag{7}$$

where ε_{ij} denotes the strain components and δ_{ij} the Kronecker delta function.

It is assumed that martensite and austenite have the same Poisson's ratio, namely $\mu_{ma}=\mu_{au}=\mu_F$[40], then the shear modulus of the SMA fiber can be obtained as

$$G_F=\frac{E_F}{2(1+\mu_F)} \tag{8}$$

where μ_F denotes the Poisson's ratio of the SMA fiber.

2 Establishment of Governing Differential Equations

2.1 Equivalent parameter formulations

Consider a SMA fiber reinforced composite beam in the Cartesian coordinate system as shown in Fig.2(a). The length, the width and the thickness are presented as L, b and h, respectively. The SMA fibers are defined in the material coordinate system 1-2-3 as schematically shown in Fig.2(b). Furthermore, SMA fibers are located parallel to the material coordinate 1-axis. As shown in Fig.2(b), β is the 1-axis orientation counterclockwise from the x axis, which is named as SMA fiber laying angle in this paper. Assume that the elastic matrix material and SMA fiber are isotropic, then the non-homogeneous material properties of the FG SMA composite monolayer are obtained by the extended multi-cell micromechanics approach[42] as follows

$$E_1=E_F f_F+E_M(1-f_F) \tag{9}$$

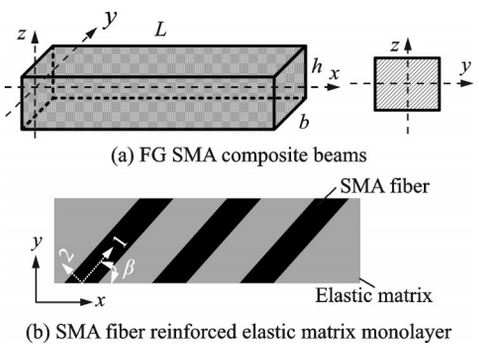

Fig.2 Schematic diagram of FG SMA composite beams and SMA fiber reinforced elastic matrix monolayer

$$E_2=E_M\left[(1-\sqrt{f_F})+\frac{E_F\sqrt{f_F}}{E_F-\sqrt{f_F}(E_F-E_M)}\right] \tag{10}$$

$$G_{12}=G_{13}=G_M\left[(1-\sqrt{f_F})+\frac{G_F\sqrt{f_F}}{G_F-\sqrt{f_F}(G_F-G_M)}\right] \tag{11}$$

$$G_{23}=\frac{G_M G_F}{G_F-\sqrt{f_F}(G_F-G_M)} \tag{12}$$

$$\alpha_1=\frac{f_F\alpha_F E_F+(1-f_F)\alpha_M E_M}{E_1} \tag{13}$$

$$\alpha_2=\frac{E_M}{E_2}\left[(1-\sqrt{f_F})\alpha_M+E_F\frac{\sqrt{f_F}\,\alpha_M-f_F(\alpha_M-\alpha_F)}{E_F-\sqrt{f_F}(E_F-E_M)}\right] \tag{14}$$

$$\mu_{12}=\mu_F f_F+\mu_M(1-f_F) \tag{15}$$

$$\mu_{21}=\frac{E_1}{E_2}\mu_{12} \tag{16}$$

where E_M, G_M, μ_M and α_M stand for the Young's modulus, the shear modulus, the Poisson's ratio and the thermal expansion coefficient of the elastic matrix, respectively; f_F denotes the volume fraction of the SMA fiber. The subscript "1""2" and "3" denote the fiber direction, the in-plane transverse direction of the fiber and the out-of-plane transverse direction of the fiber, respectively [34].

2.2 Governing differential equations

According to the Timoshenko beam theory, the displacement components can be written as

$$\begin{cases}u=u_0-z\theta\\ w=w_0\end{cases} \tag{17}$$

where u_0 and w_0 are the axial and the transverse displacements of a point on the middle plane of the beam, respectively; θ is the rotation angle; and z the distance of a point on the transverse section from the middle plane of the beam. Hence, the non-zero strains for the beam can be given by

$$\begin{cases}\varepsilon_x=u_{0,x}-z\theta_{,x}\\ \gamma_{zx}=w_{0,x}-\theta\end{cases} \tag{18}$$

where the subscript "$,x$" denotes the differentiation with respect to x.

Based on the composite laminate plate theory, the constitutive relation for the thin layer of the FG

SMA composite beam with distance z from the middle plane is considered as[35-36]

$$\sigma_x^{(z)}=\bar{Q}_{11}^{(z)}(\varepsilon_x^{(z)}-\alpha_x^{(z)}\Delta T)-\bar{Q}_{12}^{(z)}\alpha_y^{(z)}\Delta T-\bar{Q}_{15}^{(z)}\alpha_{xy}^{(z)}\Delta T-f_{\mathrm{F}}E_{\mathrm{F}}\xi\varepsilon_{\mathrm{tr}}l_x^2 \tag{19a}$$

$$\tau_{xz}^{(z)}=\bar{Q}_{44}^{(z)}\gamma_{xz}^{(z)} \tag{19b}$$

where

$$\begin{cases}\alpha_x^{(z)}=\alpha_1^{(z)}l_x^2+\alpha_2^{(z)}l_y^2\\ \alpha_y^{(z)}=\alpha_1^{(z)}l_y^2+\alpha_2^{(z)}l_x^2\\ \alpha_{xy}^{(z)}=2(\alpha_1^{(z)}-\alpha_2^{(z)})l_xl_y\end{cases} \tag{20}$$

$$\begin{cases}l_x=\cos\beta\\ l_y=\sin\beta\end{cases} \tag{21}$$

The stiffness matrix[37] can be expressed as

$$\bar{\boldsymbol{Q}}^{(z)}=\boldsymbol{T}_z\boldsymbol{Q}_z\boldsymbol{T}_z^{\mathrm{T}} \tag{22}$$

where

$$\boldsymbol{Q}_z=\begin{bmatrix}\dfrac{E_1}{1-\mu_{12}\mu_{21}} & \dfrac{\mu_{12}E_1}{1-\mu_{12}\mu_{21}} & 0 & 0 & 0\\ \dfrac{\mu_{21}E_2}{1-\mu_{12}\mu_{21}} & \dfrac{E_2}{1-\mu_{12}\mu_{21}} & 0 & 0 & 0\\ 0 & 0 & G_{12} & 0 & 0\\ 0 & 0 & 0 & G_{13} & 0\\ 0 & 0 & 0 & 0 & G_{23}\end{bmatrix} \tag{23}$$

where $\boldsymbol{Q}$ denotes the reduction stiffness matrix, and

$$\boldsymbol{T}_z=\begin{bmatrix}l_x^2 & l_y^2 & -2l_xl_y & 0 & 0\\ l_y^2 & l_x^2 & 2l_xl_y & 0 & 0\\ l_xl_y & -l_xl_y & l_x^2-l_y^2 & 0 & 0\\ 0 & 0 & 0 & l_x & l_y\\ 0 & 0 & 0 & -l_y & l_x\end{bmatrix} \tag{24}$$

where $\boldsymbol{T}_z$ denotes the coordinate transformation matrix.

In this paper, the sum algorithm of the overall stiffness matrix in the traditional laminate plate theory is improved into an integral form. Hence, the stiffness matrix of the FG SMA composite beam is given as

$$\begin{cases}\boldsymbol{A}=\displaystyle\int_{-\frac{h}{2}}^{\frac{h}{2}}\bar{\boldsymbol{Q}}^{(z)}\mathrm{d}z\\ \boldsymbol{B}=\dfrac{1}{2}\displaystyle\int_{-\frac{h}{2}}^{\frac{h}{2}}\bar{\boldsymbol{Q}}^{(z)}[(z+\mathrm{d}z)^2-z^2]\\ \boldsymbol{D}=\dfrac{1}{3}\displaystyle\int_{-\frac{h}{2}}^{\frac{h}{2}}\bar{\boldsymbol{Q}}^{(z)}[(z+\mathrm{d}z)^3-z^3]\end{cases} \tag{25}$$

The higher-order term in Eq.(25) is omitted, and it is rewritten as

$$(\boldsymbol{A},\boldsymbol{B},\boldsymbol{D})=\int_{-\frac{h}{2}}^{\frac{h}{2}}\bar{\boldsymbol{Q}}^{(z)}(1,z,z^2)\,\mathrm{d}z \tag{26}$$

In view of Eq.(26), substituting Eq.(8) into Eq.(19) and integrating Eq.(19) along the height of the beam cross section, it yields

$$A_{11}u_{0,x}-B_{11}\theta_{,x}-\int_{-\frac{h}{2}}^{\frac{h}{2}}\bar{Q}_{11}^{(z)}\alpha_x^{(z)}\Delta T\mathrm{d}z-\int_{-\frac{h}{2}}^{\frac{h}{2}}\bar{Q}_{12}^{(z)}\alpha_y^{(z)}\Delta T\mathrm{d}z-\int_{-\frac{h}{2}}^{\frac{h}{2}}\bar{Q}_{15}^{(z)}\alpha_{xy}^{(z)}\Delta T\mathrm{d}z-N_x=0 \tag{27a}$$

$$A_{44}(w_{0,x}-\theta)-Q=0 \tag{27b}$$

In view of Eq.(26), substituting Eq.(8) into Eq.(19a) and taking the moment about the neutral plane, it yields

$$B_{11}u_{0,x}-D_{11}\theta_{,x}-\int_{-\frac{h}{2}}^{\frac{h}{2}}\bar{Q}_{11}^{(z)}z\alpha_x^{(z)}\Delta T\mathrm{d}z-\int_{-\frac{h}{2}}^{\frac{h}{2}}\bar{Q}_{12}^{(z)}z\alpha_y^{(z)}\Delta T\mathrm{d}z-\int_{-\frac{h}{2}}^{\frac{h}{2}}\bar{Q}_{15}^{(z)}z\alpha_{xy}^{(z)}\Delta T\mathrm{d}z-M_x=0 \tag{27c}$$

where N_x, M_x, Q stand for the axial resultant force, the resultant moment and the resultant shear force in the FG SMA composite beam section due to the applied force, respectively. The differential Eq.(27) describes the bending deformation of FG SMA Timoshenko beams.

It should be noted that the governing differential Eq.(27) can be solved by the direct integration method. Plugging Eq.(27a) into Eq.(27c) and integrating them with respect to x yields

$$\theta=\frac{A_{11}}{(A_{11}D_{11}-B_{11}^2)}\int\left\{\frac{B_{11}}{A_{11}}N_x-M_x+\int_{-\frac{h}{2}}^{\frac{h}{2}}\left(\frac{B_{11}}{A_{11}}-z\right)[\bar{Q}_{11}^{(z)}\alpha_x^{(z)}+\bar{Q}_{12}^{(z)}\alpha_y^{(z)}+\bar{Q}_{15}^{(z)}\alpha_{xy}^{(z)}]\Delta T\mathrm{d}z\right\}\mathrm{d}x+c_1 \tag{28}$$

$$u_0=\frac{B_{11}}{(B_{11}^2-A_{11}D_{11})}\int\left\{\frac{D_{11}}{B_{11}}N_x-M_x+\int_{-\frac{h}{2}}^{\frac{h}{2}}\left(\frac{D_{11}}{B_{11}}-z\right)[\bar{Q}_{11}^{(z)}\alpha_x^{(z)}+\bar{Q}_{12}^{(z)}\alpha_y^{(z)}+\bar{Q}_{15}^{(z)}\alpha_{xy}^{(z)}]\Delta T\mathrm{d}z\right\}\mathrm{d}x+c_2 \tag{29}$$

where c_1 and c_2 are unknown constant coefficients, which can be determined in view of the boundary

conditions. Substituting Eq.(28) into Eq.(27b) and integrating them with respect to x yields

$$w_0 = \int\left(\frac{Q}{A_{44}} + \theta\right)\mathrm{d}x + c_3 \tag{30}$$

where c_3 is an unknown constant coefficient, which can also be determined in view of the boundary conditions.

For validating the mentioned method in this work, some numerical simulations on the mechanical and transformation behaviors of FG SMA composite beams subjected to a concentrated load with simply supported and clamped-free boundary conditions are transmitted and delivered in the succeeding section.

3 Numerical Simulations and Analysis

As shown in Fig.3, the FG SMA composite Timoshenko beam with two different boundary conditions, such as clamped-free and simply supported boundary conditions, are assumed. The mathematical expression of these types of boundary conditions may be written as follows.

Simply supported boundary condition

$$w_0 = 0;\ M_x = 0;\ N_x = 0;\ x = 0, L \tag{31a}$$

and

$$\theta = 0 \tag{31b}$$

at the loading position.

Clamped-free boundary condition

$$\theta = 0;\ w_0 = 0;\ x = 0 \tag{32a}$$

$$M_x = 0;\ N_x = 0;\ x = L \tag{32b}$$

For the clamped-free boundary condition, as shown in Fig.3(a), the left end of the composite beam is fixed and the right end is subjected to a concentrated force P. The axial resultant force, the resultant moment and the resultant shear force in the FG SMA composite beam section due to the applied force P can be written as

$$\begin{cases} N_x = 0 \\ M_x = P(L - x) \\ Q = -P \end{cases} \tag{33}$$

The rotation angle and transverse deflection of the FG SMA composite cantilever beam can be obtained by plugging Eqs.(32,33) into Eqs.(28,30).

For the simply supported boundary condition, a FG SMA composite simply supported beam is under a concentrated load as shown in Fig.3(b). The distance between the loading point and the left end of the beam is a. The axial resultant force, the resultant moment and the resultant shear force in the FG SMA composite beam section due to the applied force P can be written as

$$\begin{cases} N_x = 0 \\ M_x = \dfrac{P(L-a)x}{L} \\ Q = \dfrac{P(L-a)}{L} \end{cases} \quad x < a \tag{34a}$$

$$\begin{cases} N_x = 0 \\ M_x = \dfrac{P(L-a)a}{L} - \dfrac{Pa}{L}(x-a) \\ Q = -\dfrac{Pa}{L} \end{cases} \quad x > a \tag{34b}$$

The rotation angle and the transverse deflection of the FG SMA composite simply supported beam can be obtained by plugging Eqs.(31,34) into Eqs.(28,30).

For both boundary conditions, the volume fraction of SMA fiber varies continuously through the thickness of the beam and obey a power-law type of graded function as given by

$$f_{\mathrm{F}}(z) = \left(\frac{2z + h}{2h}\right)^k \tag{35}$$

where the non-negative parameter k is the power-law index that dictates the material component variation profile through the thickness of the FG SMA composite beam, which is defined as the FG parameter in this paper.

The geometric size of the FG SMA composite

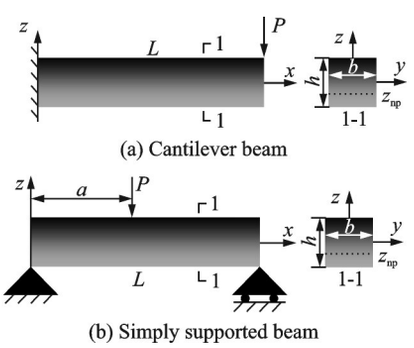

Fig.3 Schematic diagram of FG SMA composite subjected to a concentrated load

beam is L=500 mm, h=100 mm and b=50 mm. Besides, the material properties of matrix material and SMA are provided in Table 1 and Table 2, respectively.

Table 1 Material parameters of matrix[40]

E_M/GPa	μ_M	$\alpha_M/(10^{-6}\cdot(℃)^{-1})$
380	0.33	7.4

Table 2 Material parameters of SMA[40]

E_{au}/GPa	E_{ma}/GPa	μ	$\varepsilon_{tr}/10^{-2}$	$\alpha_{au}/(10^{-6}\cdot(℃)^{-1})$	$\alpha_{ma}/(10^{-6}\cdot(℃)^{-1})$
70	70	0.33	6.7	11.4	9.4
M_s /℃	A_f /℃	σ_{scr}/MPa	σ_{fcr}/MPa	$C_{ma}/(\text{MPa}\cdot(℃)^{-1})$	T_0 /℃
18.4	49	100	170	8	25

Next, the martensitic transformation and bending behavior of FG SMA composite beams with two different boundary conditions are simulated and analyzed. The concentrated load is set as −20 kN, the FG parameter k as 1, the ambient temperature T as 50 ℃ and the fiber laying angle β as 0°.

In view of boundary condition Eq.(32) and the martensitic volume fraction Eq.(4), the critical heights for the transformation starting and finishing of the FG SMA composite cantilever beam can be obtained by substituting Eqs.(28—30, 33) into Eqs.(18, 7). The height of neutral plane can be determined with the equivalent strain Eq.(7) being zero. Fig.4(a) shows the distribution patterns of martensitic volume fraction in the beam section and Fig.4(b) shows the height distribution curves of the neutral plane and martensitic transformation critical layers along the axial direction of the FG SMA composite cantilever beam(shown in Fig.3(a)).

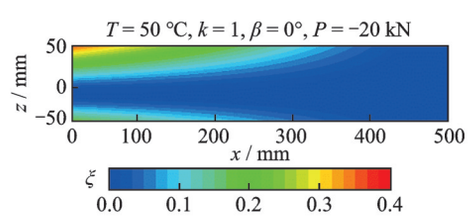

(a) Distribution pattern of martensitic volume fraction

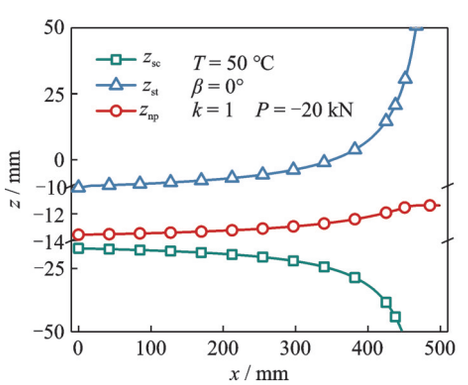

(b) Height distribution curves of the neutral plane

Fig.4 Martensitic and neutral plane of the FG SMA composite cantilever beam with P = −20 kN

As can be seen from Fig.4(a), when the concentrated end load P is −20 kN, the part of the SMA fiber in the cantilever beam has undergone an incompletely martensitic transformation. The martensitic volume fraction distribution in the cantilever beam section is asymmetrically along the z axis, and it is larger in the SMA fiber on the tension side than that on the compressive side of the cantilever beam. The position of the neutral plane does not coincide with that of the middle plane, which is the result of the graded distribution of SMA fiber along the beam thickness.

It can be seen from Fig.4(b) that the FG SMA composite cantilever beam is divided into three sections along the axial direction when the concentrated end load P is −20 kN. At the free end of the cantilever beam, no martensitic transformation occurs in the SMA fiber, and the height of the neutral plane z_{np} remains to be −11.37 mm. The critical position for the martensitic transformation starting in the SMA fiber on the upper surface is x = 466 mm, while the critical position for the martensitic transformation starting in the SMA fiber on the bottom surface is x = 447 mm. From the critical position where the martensitic transformation occurs to the fixed end of the cantilever beam, the height of the martensitic transformation starting critical layer under the tensile condition z_{st} decreases, while the height of the martensitic transformation starting critical layer under the compressive condition z_{sc} increases along the axial direction. Due to the incompletely martensitic transformation in the SMA fiber, the height of the neutral plane z_{np} gradually decreases and then tends to be stabilized from the critical posi-

tion where the martensitic transformation occurring to the fixed end of the cantilever beam.

In view of boundary condition Eq.(31) and martensitic volume fraction Eq.(4), substituting Eqs.(28—30, 34) into Eqs.(18, 7), the critical heights for the transformation starting and finishing of the FG SMA composite simply supported beam can be obtained. Fig. 5 shows the distribution patterns of martensitic volume fraction in the section of the FG SMA composite simply supported beam (shown in Fig.3(b)) with the distance between the loading point and the left end of the beam $a = L/4$ and $a = L/2$, respectively.

It can be found from Fig.5(a) that the martensitic volume fraction distribution in the simply supported beam section is asymmetrical about the loading position with $a = L/4$, and it is larger in the right side than that in the left side of the loading position. As can be seen from Fig.5(b), the martensitic volume fraction distribution in the simply supported beam section is symmetrical about the loading position with $a = L/2$. The martensitic volume fraction distribution in the simply supported beam section is asymmetrical along the z axis, and it is larger in the SMA fiber on the compressive side than that on the tensile side of the simply supported beam. The position of the neutral plane does not coincide with that of the middle plane, which is the result of the graded distribution of SMA fiber along the beam thickness.

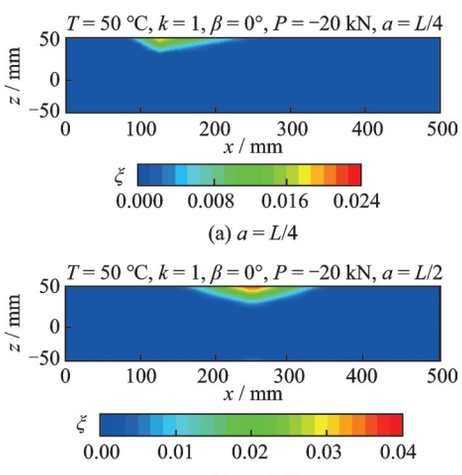

Fig.5 Distribution of martensitic volume fraction in FG SMA composite simply supported beam with $a = L/4$ and $a = L/2$

Fig.6 show the height distribution curves of the neutral plane and martensitic transformation critical layers along the axial direction of the FG SMA composite simply supported beam when a is $L/4$ and $L/2$, respectively.

As can be seen from Fig.6, no martensitic transformation occurs in the SMA fiber at the supported ends of the beam, and the height of the neutral plane z_{np} remains −11.37 mm. The critical positions for the martensitic transformation starting in the SMA fiber on the upper surface are $x = 78$ mm and $x = 266$ mm, while the critical positions for the martensitic transformation starting in the SMA fiber on the bottom surface are $x = 120$ mm and $x = 141$ mm with $a = L/4$. The critical positions for the martensitic transformation starting in the SMA fiber on the upper surface are $x = 135$ mm and $x = 365$ mm, while the critical positions for the martensitic transformation starting in the SMA fiber on the

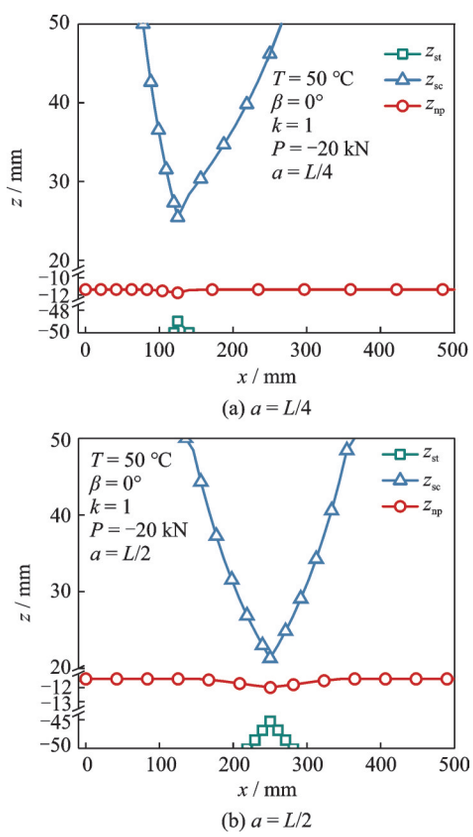

Fig.6 Curves of heights of the neutral plane and martensitic transformation critical layers along the axial direction of the FG SMA composite simply supported beam with $a = L/4$ and $a = L/2$

bottom surface are $x = 219$ mm and $x = 281$ mm with $a = L/2$.

It is obvious that from the critical position where the martensitic transformation occurs to the loading position, the height of the martensitic transformation starting critical layer in tensile condition z_{st} increases while the height of the martensitic transformation starting critical layer in compressive condition z_{sc} decreases along the axial direction. Due to the incompletely martensitic transformation in the SMA fiber, the height of the neutral plane z_{np} gradually decreases from the critical position where the martensitic transformation occurs to the lading position of the simply supported beam before the completely martensitic transformation occurs in the beam.

In view of boundary condition Eqs.(31, 32), the deflection and rotation angle of the FG SMA composite simply supported beam can be obtained by plugging Eq.(34) into Eqs.(28, 30), while the deflection and rotation angle of the FG SMA composite cantilever beam can be obtained by plugging Eq.(33) into Eqs.(28,30), respectively.

Fig.7 shows the deflection curves of the FG SMA composite beams with two different boundary conditions. Among the curves in Fig.7, it is obvious that the deflection curve of the FG SMA composite cantilever beam forms a semi-arch shape whose peak occurs in the free end. The deflection curve of the FG SMA composite simply supported beam forms a sinusoidal hump whose peak occurs at the loading position.

Fig.8 shows the rotation angle curves along the axial direction of the FG SMA composite beams with two different boundary conditions. As can be seen in Fig.8, the rotation angle curve of the FG SMA composite cantilever beam forms a semi-arch shape whose peak occurs in the free end. The rotation angle curve of the FG SMA composite simply supported beam is presented with a wave-shape form, in which the critical position for the rotation angle being zero coincides with the loading position.

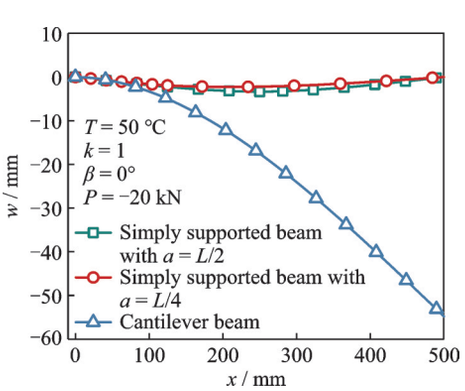

Fig.7 Deflection curves of FG SMA composite beams with two different boundary conditions

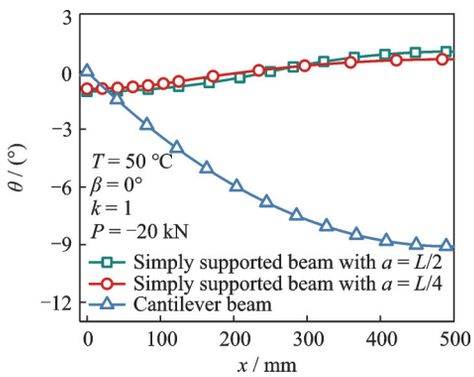

Fig.8 Rotation angle curves along the axial direction of FG SMA composite beams with two different boundary conditions

To verify the influence of the FG parameter, ambient temperature and SMA fiber laying angle, a FG SMA composite cantilever beam subjected to a concentrated end load is then analyzed.

3.1 Influence of FG parameter

The FG parameter is an important factor for the design and optimization of FG SMA composite beams. And the influence of FG parameter on the thermo-mechanical behaviors of the FG SMA composite cantilever beam is numerically investigated in this section. The concentrated end load P is -20 kN, the ambient temperature is 50 ℃ and the SMA fiber laying angle β is 0°.

Fig.9 shows the volume fraction distribution of SMA fiber along the thickness of the FG SMA composite cantilever beam with respect to different values of FG parameter k. The height curves of neutral plane and martensitic transformation critical layers along the axial direction, deflection and rotation angle curves of the FG SMA composite cantilever beam with respect to different values of FG parameter k are presented in Figs.10—13.

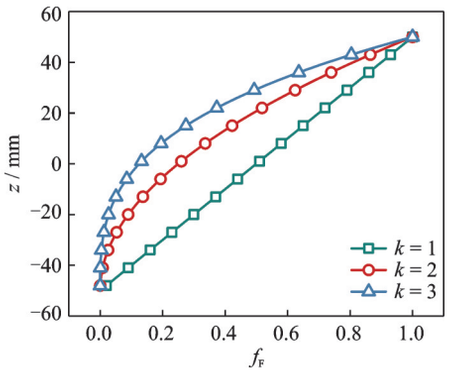

Fig.9 Volume fraction distribution of SMA fiber along the thickness of the FG SMA composite cantilever beam with respect to different FG parameters

Fig.10 shows the height curves of the neutral plane z_{np} along the axial direction of the FG SMA composite cantilever beam with respect to different values of FG parameter k. It is found that no martensitic transformation occurs in the SMA fiber at the free end of the beam in all cases. The heights of the neutral plane z_{np} remain −11.37 mm, −9.07 mm and −7.39 mm at the free end of the cantilever beam while the FG parameter k is set to be 1, 2 and 3, respectively. And the height of the neutral plane of the beam increases with the increase of FG parameter k. In all curves, the height of the neutral plane z_{np} first remains constant, then decreases, and finally tends to be stabilized from the free end to the fixed end of the cantilever beam.

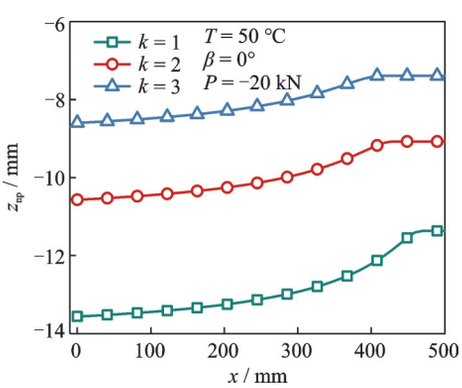

Fig.10 Curves of height of the neutral plane of the FG SMA composite cantilever beam with respect to different FG parameters

Figs.11 shows the height distribution curves of martensitic transformation starting critical layers along the axial direction of the FG SMA composite cantilever beam with respect to different values of FG parameter k.

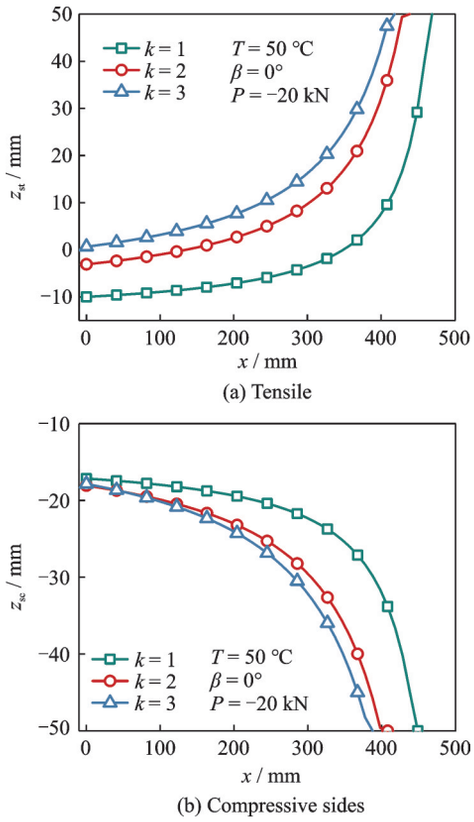

Fig.11 Curves of heights of martensitic transformation starting critical layers of the FG SMA composite cantilever beam in tensile and compressive sides with respect to different FG parameters

As can be seen from Fig.11(a), the upper surface of the FG SMA composite cantilever beam, which is in tensile state, is divided into two regions along the axial direction, including the non-transformed region and the partly transformed region. The critical coordinates for martensitic transformation starting in the SMA fiber on the upper surface are 466 mm, 439 mm and 418 mm and the heights of the martensitic transformation starting critical layer in tensile state z_{st} are −9.97 mm, −3.07 mm and 0.66 mm while the FG parameter k is set to be 1, 2 and 3, respectively.

As can be seen from Fig.11(b), the bottom surface of the FG SMA composite cantilever beam, which is in compressive state, is also divided into two regions along the axial direction. The critical coordinates for martensitic transformation starting in the SMA fiber on the bottom surface are 447 mm,

408 mm and 387 mm and the heights of the martensitic transformation starting critical layer in tensile state z_{st} are −17.15 mm, −18.09 mm and −17.86 mm while the FG parameter k is set to be 1, 2 and 3, respectively.

It can be concluded that the FG effects of martensitic transformation behavior in SMA fibers are obvious. The area of the martensitic transformed region and the martensitic volume fraction in SMA fibers all decrease with the increase of FG parameter k.

Fig.12 indicates the deflection curves of FG SMA composite cantilever beam with respect to different values of FG parameter k. Furthermore, rotation angle along the axial direction of the FG SMA composite cantilever beam with respect to different values of FG parameter k is examined through Fig.13.

It can be obviously seen from the curves in Figs.12, 13 that each curve of the deflection and rotation angle of the FG SMA composite cantilever beam forms a different semi-arch shape whose peak occurs in the free end of the cantilever beam. The absolute values of the maximum deflection of the cantilever beam are 54.80 mm, 41.27 mm and 36.68 mm, and the corresponding absolute values of maximum rotation angle are 9.10°, 7.22° and 6.42° while the FG parameter k is 1, 2 and 3, respectively. It is concluded that the FG effect of the bending behavior of the FG SMA composite cantilever beam is obvious. The absolute value of the deflection and rotation angle of the FG SMA composite cantilever beam all decrease with the increase of FG parameter k. This illustrates that the larger the value of FG parameter is, the stiffer the FG SMA composite cantilever beam is.

It can be noticed from above mentioned simulation and discussion that the FG parameter k has a significant effect on the martensitic transformation and bending deformation of the FG SMA composite beam and therefore the static bending deformation may be controlled by choosing an appropriate value of k. For the sake of simplicity, the FG parameter k is set to be 1 in the following numerical examples.

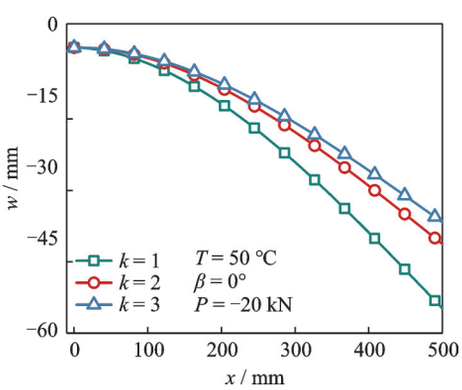

Fig.12 Deflection curves of the FG SMA composite cantilever beam with respect to different FG parameters

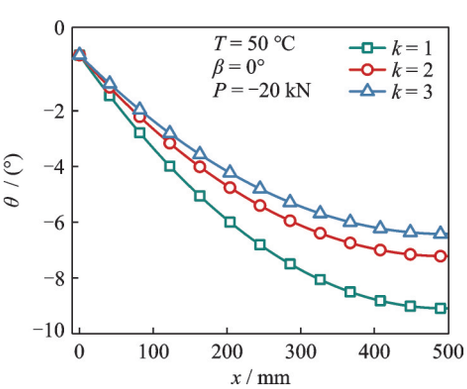

Fig.13 Rotation angle curves along the axial direction of the FG SMA composite cantilever beam with respect to different FG parameters

3.2 Influence of ambient temperature

In order to study the influence of ambient temperature on the bending behavior of the FG SMA composite cantilever beam, the deflection and rotation angle curves of the cantilever beam with different ambient temperatures are presented in Figs.14, 15, respectively. The concentrated end load P is −20 kN, and the SMA fiber laying angle β is 0°.

It can be obviously seen from the curves in

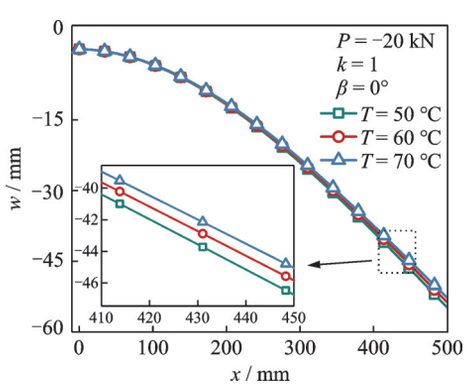

Fig.14 Deflection curves of FG SMA composite cantilever beam with different ambient temperatures

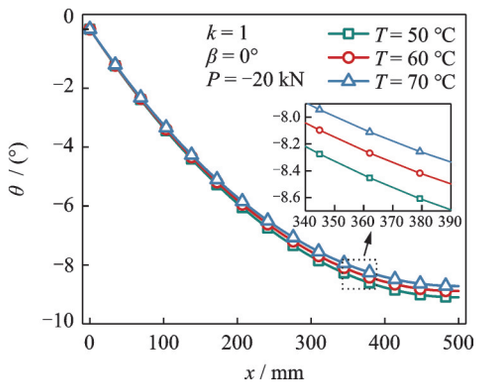

Fig.15 Rotation angle curves along the axial direction of the FG SMA composite cantilever beam with different ambient temperatures

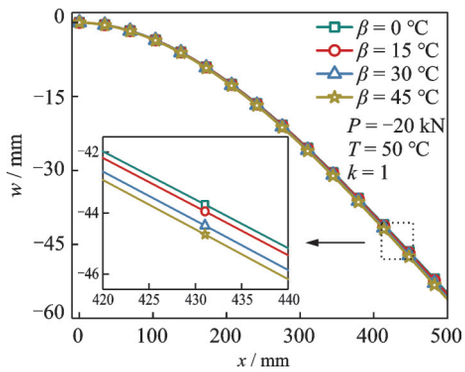

Fig.16 Deflection curves of FG SMA composite cantilever beam with different fiber laying angles

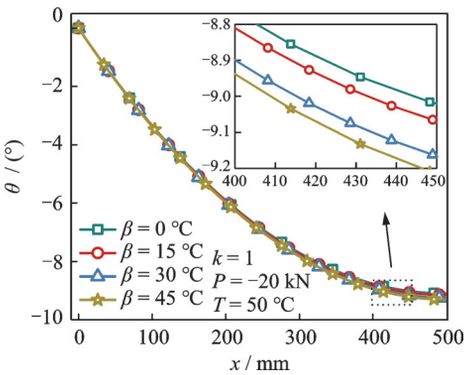

Fig.17 Rotation angle curves along the axial direction of the FG SMA composite cantilever beam with different fiber laying angles

Figs. 14, 15 that the absolute values of the maximum deflection of the cantilever beam are 54.80 mm, 53.72 mm and 52.77 mm, and the corresponding absolute values of maximum rotation angle are 9.10°, 8.89° and 8.72°, when the ambient temperatures are 50 ℃, 60 ℃ and 70 ℃, respectively. This illustrates that with the increase of ambient temperature, the absolute value of the deflection and rotation angle of the FG SMA composite cantilever beam decreases and stiffness of the cantilever beam increases. This is because that the critical martensitic transformation stresses increase with the increase of ambient temperature, which leads to a smaller martensitic transformation strain in the SMA fiber at the same stress level.

3.3 Influence of fiber laying angle

In order to study the influence of SMA fiber laying angle on the bending behavior of the FG SMA composite cantilever beam, the deflection and rotation angle curves of the cantilever beam with different SMA fiber laying angles are presented in Figs.16, 17. The concentrated end load P is −20 kN, and the ambient temperature is 50 ℃.

As can be seen from the curves in Figs.16, 17, the absolute values of the maximum deflection of the cantilever beam are 54.80 mm, 55.10 mm, 55.70 mm and 56.08 mm, and the corresponding absolute values of maximum rotation angle are 9.10°, 9.14°, 9.25° and 9.31°, while the SMA fiber laying angles are 0°, 15°, 30° and 45°, respectively. It is concluded that the influence of fiber laying angle on the deflection and rotation angle of the FG SMA composite cantilever beam is not obvious, and the influence of the SMA fiber laying angle can be neglected in designing the smart beam structures.

4 Conclusions

A thermo-mechanical investigation on the function graded shape memory alloy (FG SMA) Timoshenko composite beams is presented by considering the shear deformation and thermal effect. The volume fraction of the SMA fiber is assumed to vary along the thickness according to a power-law type function, and the equivalent parameters of the FG SMA composite beam are obtained by the extended multi-cell micromechanics approach. The governing differential equations are established by the composite laminated plate theory, and the martensitic transformation and bending deformation of FG SMA composite beams subjected to a concentrated load with two different boundary conditions are numeri-

cally simulated. Furthermore, the influences of FG parameter, ambient temperature and SMA fiber laying angle on the martensitic transformation and bending deformation of FG SMA composite beams are numerically analyzed. Some important conclusions are summarized as follows:

(1) The graded distribution of SMA fiber volume fraction along the beam thickness results in that the position of the neutral plane does not coincide with that of the middle plane. The height of the neutral plane remains constant in the non-transformed region and decreases to be stable in the partly transformed region, but increases in the completely transformed region of SMA fiber.

(2) The FG parameter has a significant effect on the martensitic transformation and bending deformation of the FG SMA composite beam. The area of the martensitic transformed region and the martensitic volume fraction in SMA fiber all decrease with the increased value of FG parameter. The larger the value of FG parameter is, the stiffer the FG SMA composite beam is.

(3) The ambient temperature is an important factors related to the martensitic transformation of SMA fiber and bending deformation of the FG SMA composite beam. With the ambient temperature increases, the absolute value of deflection and the rotation angle of the FG SMA composite beam decrease and the stiffness of the FG SMA composite beam increases.

(4) The influence of SMA fiber laying angle on the martensitic transformation of SMA fiber and bending deformation of the FG SMA composite beam is not obvious and can be negleted.

References

[1] ZHAO L, CHEN W Q, LU C F. Symplectic elasticity for bi-directional functionally graded materials[J]. Mechanics of Materials, 2012, 54: 32-42.

[2] NAEBE M, SHIRVANIMOGHADDAM K. Functionally graded materials: A review of fabrication and properties[J]. Applied Materials Today, 2016, 5: 223-245.

[3] SUN Y H, CHENG J H, WANG Z G, et al. Analytical approximate solution for nonlinear behavior of cantilever FGM MEMS beam with thermal and size dependency[J]. Mathematical Problems in Engineering, 2019: 1-10.

[4] MOHD-JANI J, LEARY M, SUBIC A, et al. A review of shape memory alloy research, applications and opportunities[J]. Materials and Design, 2014, 56: 1078-1113.

[5] SUN L, HUANG W M, DING Z, et al. Stimulus-responsive shape memory materials: Review[J]. Materials and Design, 2012, 33: 577-640.

[6] ZHOU B, LIU Y J, LENG J S, et al. A macro-mechanical constitutive model of shape memory alloys[J]. Science in China Series G: Physics, Mechanics and Astronomy, 2009, 52(9): 1382-1391.

[7] ZHOU B. A macroscopic constitutive model of shape memory alloy considering plasticity[J]. Mechanics of Materials, 2012, 48(4): 71-81.

[8] CISSE C, ZAKI W, ZINED T B. A review of constitutive models and modeling techniques for shape memory alloys[J]. International Journal of Plasticity, 2016, 76: 244-284.

[9] ZHENG Y, DONG Y, LI Y H. Resilience and life-cycle performance of smart bridges with shape memory alloy (SMA)-cable-based bearings[J]. Construction and Building Materials, 2018, 158: 389-400.

[10] JHOU W T, WANG C, II S, et al. TiNiCuAg shape memory alloy films for biomedical applications[J]. Journal of Alloys and Compounds, 2018, 738: 336-344.

[11] CHOUDHARY N, KAUR D. Shape memory alloy thin films and heterostructures for MEMS applications: A review[J]. Sensors and Actuators A: Physical, 2016, 242: 162-181.

[12] SHARIAT B S, LIU Y N, BAKHTIARI S. Modelling and experimental investigation of geometrically graded shape memory alloys with parallel design configuration[J]. Journal of Alloys and Compounds, 2019, 791: 711-721.

[13] KHALEGHI F, TAJALLY M, EMADODDIN E, et al. The investigation of the mechanical properties of graded high-temperature shape memory Ti-Ni-Pd alloy[J]. Journal of Alloys and Compounds, 2019, 787: 882-892.

[14] FU Y Q, DU H J, ZHANG S. Functionally graded TiN/TiNi shape memory alloy films[J]. Materials Letters, 2003, 57(20): 2995-2999.

[15] MAHMUD A S, LIU Y N, NAM T H. Design of functionally graded NiTi by heat treatment[J]. Physica Scripta, 2007, T129: 222-226.

[16] TIAN H, SCHRYVERS D, MOHANCHANDRA

K P, et al. Fabrication and characterization of functionally graded Ni-Ti multilayer thin films[J]. Functional Materials Letters, 2009, 2(2): 61-66.

[17] BIRNBAUM A J, SATOH G, YAO Y L. Functionally grading the shape memory response in NiTi films: Laser irradiation[J]. Journal of Applied Physics, 2009, 106(4): 043504-8.

[18] MAHMUD A S, LIU Y N, NAM T H. Gradient anneal of functionally graded NiTi[J]. Smart Materials and Structures, 2008, 17(1): 015031.

[19] MENG Q L, LIU Y N, YANG H, et al. Laser annealing of functionally graded NiTi thin plate[J]. Scripta Materialia, 2011, 65(12): 1109-1112.

[20] MENG Q L, LIU Y N, YANG H, et al. Functionally graded NiTi strips prepared by laser surface anneal[J]. Acta Materialia, 2012, 60(4): 1658-1668.

[21] YANG S Y, KANG S W, LIM Y M, et al. Temperature profiles in a Ti-45Ni-5Cu (at%) shape memory alloy developed by the Joule heating[J]. Journal of Alloys and Compounds, 2010, 490(1/2): L28-L32.

[22] MENG Q L, YANG H, LIU Y N, et al. Compositionally graded NiTi plate prepared by diffusion annealing[J]. Scripta Materialia, 2012, 67(3): 305-308.

[23] MENG Q L, WU Z G, BAKHTIARI R, et al. A unique "fishtail-like" four-way shape memory effect of compositionally graded NiTi[J]. Scripta Materialia, 2017, 127: 84-87.

[24] SHARIAT B S, LIU Y N, RIO G. Thermomechanical modelling of microstructurally graded shape memory alloys[J]. Journal of Alloys and Compounds, 2012, 541: 407-414.

[25] SHARIAT B S, LIU Y N, RIO G. Mathematical modelling of pseudoelastic behaviour of tapered NiTi bars[J]. Journal of Alloys and Compounds, 2013, 577(1): S76-S82.

[26] SHARIAT B S, LIU Y N, RIO G. Modelling and experimental investigation of geometrically graded NiTi shape memory alloys[J]. Smart Materials and Structures, 2013, 22(2): 025030.

[27] MOHRI M, NILI-AHMADABADI M. Phase transformation and structure of functionally graded Ni-Ti bilayer thin films with two-way shape memory effect[J]. Sensors and Actuators A: Physical, 2015, 228: 151-158.

[28] MOHRI M, TAGHIZADEH M, WANG D, et al. Microstructural study and simulation of intrinsic two-way shape memory behavior of functionally graded Ni-rich/NiTiCu thin film[J]. Materials Characterization, 2018, 135: 317-324.

[29] LIU B F, WANG Q F, ZHOU R, et al. Study on behaviors of functionally graded shape memory alloy cylinder[J]. Acta Mechanica Solida Sinica, 2017, 30(6): 608-617.

[30] SHARIAT B S, MENG Q L, MAHMUD A S, et al. Functionally graded shape memory alloys: Design, fabrication and experimental evaluation[J]. Materials and Design, 2017, 124: 225-237.

[31] SHARIAT B S, BAKHTIARI R, LIU Y N. Nonuniform transformation behaviour of NiTi in a discrete geometrical gradient design[J]. Journal of Alloys and Compounds, 2019, 774: 1260-1266.

[32] SHARIAT B S, MENG Q L, MAHMUD A S, et al. Experiments on deformation behaviour of functionally graded NiTi structures[J]. Data in Brief, 2017, 13: 562-568.

[33] KHALEGHI F, TAJALLY M, EMADODDIN E, et al. The investigation of the mechanical properties of graded high- temperature shape memory Ti-Ni-Pd alloy[J]. Journal of Alloys and Compounds, 2019, 787: 882-892.

[34] SHARIYAT M, HOSSEINI S H. Accurate eccentric impact analysis of the preloaded SMA composite plates based on a novel mixed-order hyperbolic global-local theory[J]. Composite Structure, 2015, 124: 140-151.

[35] SAMADPOUR M, SADIGHI M, SHAKERI M, et al. Vibration analysis of thermally buckled SMA hybrid composite sandwich plate[J]. Composite Structure, 2015, 119: 251-263.

[36] KAMARIAN S, SHAKERI M. Thermal buckling analysis and stacking sequence optimization of rectangular and skew shape memory alloy hybrid composite plates[J]. Composites Part B, 2017, 116: 137-152.

[37] SOLTANIEH G, KABIR M Z, SHARIYAT M. A robust algorithm for behavior and effectiveness investigations of super-elastic SMA wires embedded in composite plates under impulse loading[J]. Composite Structures, 2017, 179: 355-367.

[38] SHARIAT B S, LIU Y N, MENG Q L, et al. Analytical modelling of functionally graded NiTi shape memory alloy plates under tensile loading and recovery of deformation upon heating[J]. Acta Materialia, 2013, 61(9): 3411-3421.

[39] LIU B F, DUI G S, YANG S Y. On the transformation behavior of functionally graded SMA compo-sites subjected to thermal loading[J]. European Journal of Mechanics-A/Solids, 2013, 40(1): 139-147.

[40] LIU B F, NI P C, ZHANG W. On behaviors of func-

tionally graded SMAS under thermo-mechanical coupling[J]. Acta Mechanica Solida Sinica, 2016, 29(1): 46-58.

[41] XUE L J, DUI G S, LIU B F, et al. A phenomenological constitutive model for functionally graded porous shape memory alloy[J]. International Journal of Engineering Science, 2014, 78: 103-113.

[42] ASADI H, AKBARZADEH A H, WANG Q. Nonlinear thermo-inertial instability of functionally graded shape memory alloy sandwich plates[J]. Composite Structures, 2015, 120: 496-508.

[43] LIU H W, WANG J, DAI H H. Analytical study on stress-induced phase transitions in geometrically graded shape memory alloy layers. Part I: Asymptotic equation and analytical solutions[J]. Mechanics of Materials, 2017, 112: 40-55.

[44] BRINSON L C. One-dimensional constitutive behavior of shape memory alloys: Thermomechanical derivation with non-constant material functions and redefined martensite internal variable[J]. Journal of Intelligent Materials Systems and Structures, 1993, 4(2): 229-242.

[45] ZHOU B, YOON S H, LENG J S. A three-dimensional constitutive model for shape memory alloy[J]. Smart Materials and Structures, 2009, 18(9): 095016.

Authors Prof. **ZHOU Bo** received the B.S. degree in engineering mechanics from Dalian University of Technology in 1995 and Ph.D. degree in mechanical engineering from Kumoh National Institute of Technology in 2007. He joined China University of Petroleum (East China) in September 2012, where he is a professor of engineering mechanics. His research is focused on smart materials and structures and relevant fields.

Prof. **XUE Shifeng** received the B.S. degree in applied mechanics from Tianjin University in 1984 and Ph.D. degree in solid earth geophysics from Institute of geology of China Earthquake Administration in 2000. He joined China University of Petroleum (East China) in August 1984, where he is a professor of engineering mechanics. His research is focused on computational mechanics and relevant fields.

Author contributions Prof. **ZHOU Bo** designed the study. Dr. **KANG Zetian** wrote the manuscript. Mr. **MA Xiao** contributed the data curation. Prof. **XUE Shifeng** validated the methodology. Prof. **YANG Jie** reviewed and revised the manuscript. All authors commented on the manuscript draft and approved the submission.

Competing interests The authors declare no competing interests.

(Production Editor: ZHANG Bei)

功能梯度形状记忆合金Timoshenko复合梁的热-力学行为

周 博[1], 康泽天[1], 马 宵[1], 薛世峰[1], 杨 杰[2]

(1.中国石油大学(华东)储运与建筑工程学院, 青岛 266580, 中国;
2.皇家墨尔本理工大学工程学院, 墨尔本 3083, 澳大利亚)

摘要: 基于Timoshenko梁理论,详细研究了功能梯度(Functionally graded,FG)形状记忆合金(Shape memory alloy,SMA)复合梁的热-力学行为。考虑SMA纤维体积分数按幂律函数沿梁厚度方向呈连续梯度变化,并给出了相应的等效参数。采用复合材料层合板理论,建立了可直接积分求解的控制微分方程。数值分析了不同边界条件下,FG参数、环境温度和SMA纤维铺设角度对复合梁的热-力学行为的影响。研究结果表明,复合梁的中性面位置与中面位置不重合,且SMA马氏体沿梁厚度方向不均匀分布。FG参数和环境温度的增加均增大了复合梁的刚度,而SMA纤维铺设角度的影响可以忽略不计。本工作为FG SMA结构的设计和应用提供了理论依据。

关键词: 形状记忆合金;剪切变形;热效应;层合板理论;功能梯度梁